Rare Palaeomagnetic Evidence of Long-term Mantle Control of the Geodynamo and Possible Role of the NAD-field in the Reversal Process

Kenneth A Hoffman, Pierre Camps, Matt Carlton

Geophysical Journal International

Geophys. J. Int. (2019) **221,** 142–150
Advance Access publication 2019 October 22
GJI Geomagnetism, rock magnetism and palaeomagnetism

doi: 10.1093/gji/ggz480

Rare palaeomagnetic evidence of long-term mantle control of the geodynamo and possible role of the NAD field in the reversal process

Kenneth A. Hoffman,[1,2] Pierre Camps[3] and Matt Carlton[4]

[1]*Physics Department, Cal Poly State University, San Luis Obispo, CA* 93407, *USA. E-mail: khoffman@calpoly.edu*
[2]*Department of Geoscience, University of Wisconsin-Madison, Madison, WI* 53706, *USA*
[3]*Géosciences Montpellier, Universite de Montpellier, 34090 Montpellier, Languedoc-Roussillon, France*
[4]*Statistics Department, Cal Poly State University, San Luis Obispo, CA* 93407, *USA*

Accepted 2019 October 20. Received 2019 October 17; in original form 2019 April 16

SUMMARY

The degree to which the lowermost mantle influences behaviour of the geodynamo has been debated over the past quarter century. Our analysis of a comprehensive set of 17 Cenozoic palaeomagnetic transitional field records obtained from lavas in the Southern Hemisphere provides robust evidence of stable mantle control since the Pliocene. The records come from a region where—given a significantly weakened axial dipole—the magnetic field *today* would be largely controlled by the non-axial dipole (NAD) flux patch currently emanating from Earth's outer core beneath western Australia. The palaeomagnetic recording sites from west to east include the south Indian Ocean, eastern Australia, New Zealand and French Polynesia. The analysed records contain from 2 to 26 sequential transitional virtual geomagnetic poles (VGPs). 10 of the 17 records supply at least one VGP within a narrow longitudinal band 10°-wide between 60°S and the equator, centred along 102.4°E. That is, transitional data from 59 per cent of the Cenozoic recordings are found to reside in a region that encompasses a mere 2.8 per cent of the VGP transitional area on Earth's surface. A robust Monte Carlo approach applied to this data set, one that takes into account the number of transitional VGPs contained in each record, finds this result highly improbable ($p\text{-value} = 0.0006$). The present-day pattern of vertical flux at the core–mantle boundary shows an anomalously strong, thin Southern Hemisphere longitudinal band off the west coast of Australia that strikingly coincides with this unusual palaeomagnetic finding. We conclude with a high degree of confidence that this band of flux has remained virtually unmoved for at least the past 3 Myr. Seemingly independent of the behaviour of the axial dipole, our findings indicate that it has dominated the magnetic field over an area of considerable size during attempts by the geodynamo to reverse polarity.

Key words: Palaeomagnetism; Geomagnetic reversal; Geomagnetic field; Core dynamics; Core-mantle boundary; Dynamo theory.

1 INTRODUCTION

The claim that the lowermost mantle exerts control over the morphology of the geomagnetic field first came to light from palaeomagnetic findings showing preferred locations of transitional virtual geomagnetic poles (VGPs; e.g. Laj *et al.* 1991; Hoffman 1992). Further support for the idea came from correlations of the palaeomagnetic findings with aspects of the modern-day non-axial dipole (NAD) field and lower-mantle seismic tomography (e.g. Constable 1992; Hoffman 1992). In particular, studies of Cenozoic lava sequences about the globe that recorded field behaviour during times of transition contain clusters, or groupings, of transitional VGPs at particular recurring localities (e.g. Hoffman 1992; Brown *et al.* 2004; Bogue *et al.* 2017), and most notably off the coast of western Australia (e.g. Chauvin *et al.* 1990; Roperch & Duncan 1990; Hoffman & Singer 2004; Hoffman *et al.* 2008) as well as the antipodal region (Mochizuki *et al.* 2011).

An alternative explanation of clustered transitional VGPs is that, rather than being due to extended stands by the vector field, the clusterings are artefacts of rapid-fire volcanic eruptions (e.g. Valet & Plenier 2008). That volcanic eruptions may occur episodically, sometimes at a rapid rate, which is not debatable. Riisager *et al.* (2003) point out that one or both 'types' of VGP clusters can be present in a single transitional field record. Nonetheless, there remains some question as to whether such palaeomagnetic recurrences can ultimately prove long-term mantle control over the geodynamo. Here, we shed light on the controversy with robust data that points strongly towards the affirmative.

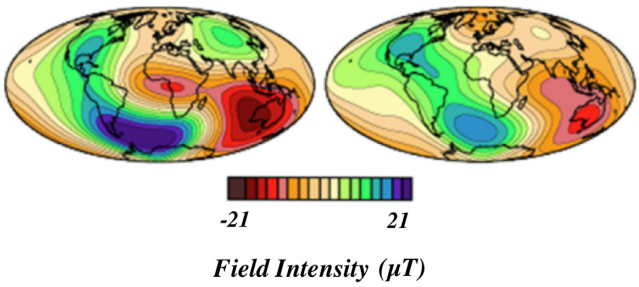

Figure 1. Vertical component of the non-axial dipole (NAD) field at Earth's surface—left: Year 2000; right: 400-yr average from 1590 to 1990 (Constable 2007a, pg. 704).

2 THE AXIAL DIPOLE (AD)—NON-AXIAL DIPOLE (NAD) FIELD DICHOTOMY

The NAD field is composed of the non-dipole field with the addition of the two equatorial dipole terms. (The NAD can also be referred to as the 'SAD field', 'S' standing for the French *sans*; hence, unambiguously 'the total field without the axial dipole term'.) The dipole contribution to the entire geomagnetic field—specifically, the axial dipole (AD) term g_1^0 determined from spherical harmonic analysis—is anomalously and uniquely strong not only at Earth's surface but also when calculated to the depth of the core–mantle boundary (CMB; e.g. Courtillot *et al*. 1992). This finding alone suggests, if not a separation of the AD-field source from that responsible for the NAD field, no less than an enhanced generative efficiency of the former by the dynamo process. Analysis of the modern-day geomagnetic NAD field (Fig. 1, left) displays four particularly discernible vertical flux concentrations at Earth's surface (see Constable 2007a)—one each in North America, the south Atlantic, Siberia and western Australia—that appear through the work of Jackson *et al*. (2000) to have remained stationary over the past 400 yr (Fig. 1, right).

Hoffman (1992) suggested that core–mantle interactions are responsible for the most intense features of the observed NAD-field flux pattern, a notion based on the apparent one-to-one correspondence with *P* -wave velocity maxima reported in Dziewonski & Woodhouse's 1987 seminal normal-mode seismic tomography study of the lower mantle (Fig. 2, top left). Recent Stoneley-mode predictions by Koelemeijer *et al.* (2017) of lowermost mantle heterogeneities (Fig. 2, top right) offer support that the state of these CMB regions are anomalous, further suggesting that NAD-field morphology almost exclusively originates by way of fluid action at shallow depths within the outer core under the influence of varied boundary conditions at the base of the mantle. Also, several shear wave tomographic models at 2800 km depth consistently show faster velocities at NAD-field maxima sites (Ritsema *et al.* 2011); two such models are seen at the bottom of Fig. 2.

This shallow-core, mantle-influenced flux pattern, however, cannot be precisely the NAD; it will also contain a non-zero contribution from the g_1^0 axial dipole term. Thus, in order to distinguish this part of the geomagnetic field appropriately we follow Hoffman & Singer (2008) and use the designation shallow core-generated (SCOR) field. Yet, since the AD field component arising from heterogeneous shallow-core conditions is likely an insignificant fraction of the total axial dipole term and difficult to quantify, we will employ well-analysed NAD-field constructions to closely approximate the SCOR in the study that follows.

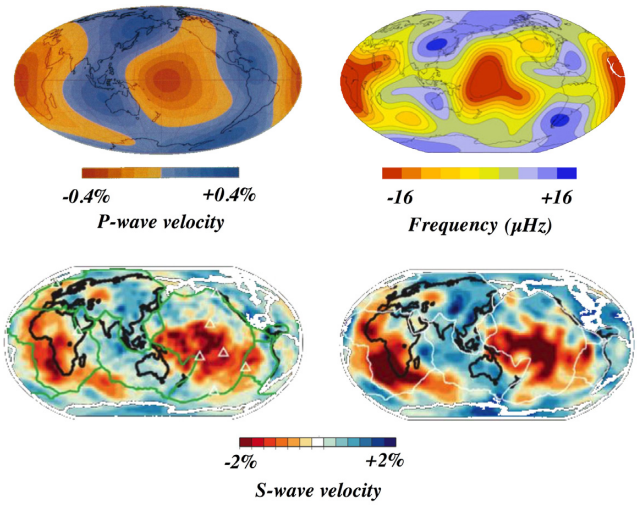

Figure 2. Top left: normal-mode analysis of *P*-wave velocity anomalies at a depth of 2300 km; blue and orange regions denoting fast and slow velocity anomalies, respectively (from Dziewonski & Woodhouse 1987, figure 9). Top right: predicted Stoneley-mode splitting of ${}_2S_{16}$ at 2800 km depth for shear-and-compressional-wave velocity model SP12RTS (from Koelemeijer *et al.* 2017, figure 2). Note in both cases the strong correspondence with primary NAD-field features in Fig. 1. (The same features, however, are not clearly predicted for Stoneley mode ${}_3S_{16}$.) Bottom: shear wave velocity anomalies for models S40RTS (Ritsema *et al.* 2011, figure 11) and S362ANI (Kustowski *et al.* 2008, figure 12). Again, fast velocity anomalies (in blue) are associated with regions of NAD-field maxima.

During the 100 yr between 1900 and 2000, the primary NAD-field flux features remained spatially fixed while varying in strength at differing rates (see Hoffman & Singer 2004). For example, in the Southern Hemisphere the rate of change in strength of the flux patch beneath western Australia outpaced the patch in the South Atlantic. This differential in flux growth causes the rate of directional secular variation due to the NAD field alone, here termed 'NAD-SV', to be strongly site-dependent about the globe. Sites near a particular flux concentration will be mainly influenced by that particular patch; will be associated with NAD-field north (or south) VGPs being strongly attracted to it; and will experience a low level of NAD-SV. Sites, say, equidistant between two flux patches will experience an influence by both; will likely be associated with NAD-field VGPs not in close proximity to either concentration; and, in general, will experience a high level of NAD-SV.

3 TRANSITIONAL FIELD RECORDS FROM THE LOW NAD-SV REGION

Fig. 3 shows a contour map of angular change of VGPs associated with the NAD field over the 20th century (Hoffman & Singer 2008). Contoured colour-coding, in increments of 5° from 0°-to-5° (dark blue) to 40°-to-45° (deep red), shows the global pattern of this angular change. We classify regions of differing degrees of NAD-SV as follows: 0°–15° of angular change as low, 15°–30° as mid-range and 30°–45° as high. The darkest blue patches—representing minimal angular change—are seen in and around North America (1), Siberia (2) and Australia (3), each near a location of strong subvertical flux. The Australian is the only patch of the four emanating upwardly directed flux, a distinction that may help to explain its extensive regional influence. Since the four NAD-field flux concentrations observed today appear to have had a dominating influence over the

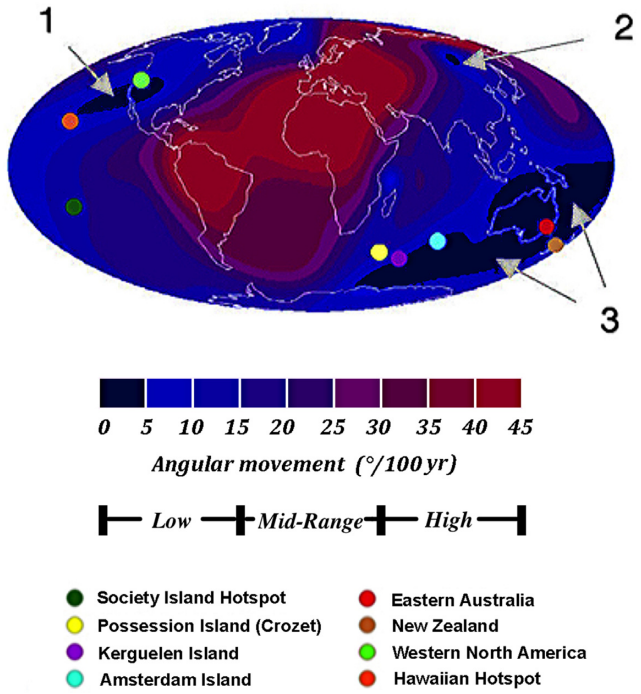

Figure 3. Contour map of angular change of VGPs associated with the NAD field over the 20th century. Deeper shades of blue and red represent lower and higher degrees, respectively, of this secular change (after Hoffman & Singer 2008). Minima (deepest shade of blue) are found along the west coast of North America (1), in Siberia (2) and throughout a sizeable region centred in Australasia (3). Superposed are blue-region sites (<15° of movement) from which lava-based transitional field records have been obtained (colour-coded as indicated).

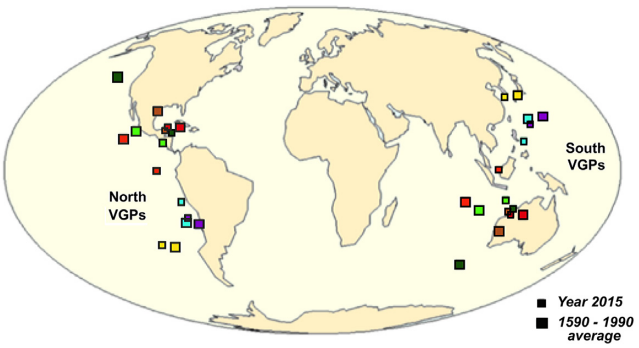

Figure 4. Calculated VGPs associated with the present-day NAD field and the average historic NAD field for the sites shown in Fig. 3. Both north VGPs and south VGPs are displayed as indicated and colour-coded corresponding to the site.

past 400 yr (Fig. 1), the question we now explore is the time over which they may have persisted.

Assume as has been suggested that during those times when the AD field was particularly weak, these flux features, especially the Australian patch, dominated the global field. Assume further that this particular patch of flux remained stably in place from the present over sufficient geologic time spanning several transitional field events. If so, then a measure of the time of its persistence may be gleaned from the palaeomagnetic record of transitional field directions. Specifically, any site on Earth's surface within or in close proximity to the large low-NAD-SV (blue) region associated with the Australian flux patch would experience palaeofield directions corresponding to either north or south VGPs (depending on sign) within or in close proximity to the flux patch, it being the primary magnetic field source.

We can test the above scenario by analysing palaeomagnetic transitional field records obtained from lava sequences at sites that today would experience a dominating effect from the Australian NAD-field flux patch given a significantly weakened AD field. We chose the Australian patch for this analysis because of its widespread significance on 20th century NAD-SV and the availability of numerous transitional field lava-based records from sites within its range of influence; we now focus our analysis on data from sites found in and about the low NAD-SV centred near western Australia.

There are eight of these 'blue-region' sites about the globe (Fig. 3) from which lava-based palaeomagnetic transitional field records have been obtained. Of these, six are in the Southern Hemisphere––in the south Pacific, Australasia and the south Indian Ocean. The remaining two sites are in the Northern Hemisphere—in western North America and at the Hawaiian hotspot.

VGPs of each sign associated with all eight blue-region sites, calculated for the present-day NAD field alone, and for the 400-yr-averaged NAD from 1590 to 1990 (Jackson *et al.* 2000), are plotted in Fig. 4. For each site, regardless of being in the Northern or Southern Hemisphere, the two VGP determinations are found in close proximity to one another. This finding provides support for the contention that the NAD flux pattern is largely controlled by quasi-static conditions in the lowermost mantle at least during historical times. The question is how far back into the geologic record can this apparent control be observed?

We exclude from our final analysis palaeomagnetic data obtained from the two Northern Hemisphere sites (e.g. Bogue & Coe 1984; Prévot *et al.* 1985; Leonhardt *et al.* 2009; Bogue *et al.* 2017). Although these sites experience some influence from the Australian flux patch, their associated NAD fields are not dominated by it. Rather, their modern-day NAD fields are far more affected by the flux concentration emanating from beneath North America, both sites being located along the periphery of the North American NAD-SV minimum (see Fig. 3).

4 TRANSITIONAL VGPs AND ANALYSIS

The six Southern Hemisphere site localities have provided in total 17 lava-based records of transitional fields spanning the last ~40 Myr of the Cenozoic (Table 1). Fig. 5 shows a compilation of 155 transitional VGPs—those which lie between 60°N and 60°S latitude—obtained from the 17 Southern Hemisphere blue-region site records. Sequences represented contain a minimum of two serially recorded transitionally magnetized lavas (Table 1). The choice of 60°—often chosen as the cut-off for transitional VGPs—is nonetheless arbitrary. There can be no universal cut-off for a transitional VGP since the relationship between directional rotation and pole migration is non-orthogonal (see Hoffman 1984a). Tectonic corrections were made for the four oldest records. A hotspot reference frame is used (see Appendix A for details) in which one implicitly assumes there to be no true polar wander since ~37 Ma—which may or may not be the case.

Since the dynamo is blind to the direction of magnetic flux lines, antipodal palaeodirections are equivalent in so far as outer core fluid dynamics is concerned. That is, virtual poles may be treated as either north-VGPs or south-VGPs. This is the so-called 'geomagnetic convention'—a procedure that has been shown to be helpful

Table 1. Transitional field records from low NAD-SV (blue-region) sites.

Lava Location	Eruption Site	Event	Age	Color	a / b*	Refs
New Zealand; North Island	Present Day Site Location	Mono Lake Excursion	~32 ka		0/13 (0%)	Cassidy (2006)
Tahiti	Society Island Hotspot	Los Tilos Event	~590 ka		6/13 (46%)	Hoffman & Singer (2004) Singer (2014)
"	"	Matuyama-Brunhes R-N	~776 ka		2/6 (33%)	Chauvin et al. (1990)
"	"	Matuyama-Brunhes R-N	~776 ka		3/6 (50%)	Mochizuki et al. (2011)
"	"	Jaramillo-Matuyama N-R	~1.00 Ma		1/23 (4%)	Chauvin et al. (1990)
"	"	Punaruu Event	~1.12 Ma		3/13 (23%)	Chauvin et al. (1990) Singer (2014)
Huahine	"	Pliocene event	~2.9 Ma		2/17 (12%) **	Roperch & Duncan (1990)
Raiatea	"	Raiatea Excursion	~2.77 Ma		0/6 (0%)	Yamamoto et al. (2007)
Taha'a	"	Mammoth R-N (?)	~3.20 Ma		0/4 (0%)	Yamamoto et al. (2007)
Amsterdam Island	Present Day Site Location	Brunhes Excursion	Late Brunhes		1/2 (50%)	Carvallo et al. (2003)
Possession (Crozet) Island	"	Normal Polarity Excursion	Pliocene		0/3 (0%)	Camps et al. (2001)
Kerguelen Island	Plate Tectonically-Corrected Oligocene Site Location***	Oligocene N-R	~28 Ma		1/4 (25%)	Plenier et al. (2002)
Queensland, Australia	Plate Tectonically-Corrected Oligocene Site Location***	Quamby Falls R-N	~26.5 Ma		5/15 (33%)	Hoffman et al. (2008)
New South Wales, Australia	Plate Tectonically-Corrected Eocene Site Location***	Liverpool R-N	~37 Ma		0/26 (0%)	Hoffman (1986)
New South Wales, Australia	Plate Tectonically-Corrected Miocene Site Location***	Mt. Kaputar Excursion	~18 Ma		0/7 (0%)	Hoffman (1986)
New Zealand: South Island	Present Day Site Location	Akaroa N-R	9.51 Ma		1/3 (33%)	Hoffman (1986)
"	"	Akaroa R-N	9.67 Ma		0/3 (0%)	Hoffman (1986)

*a/b # Southern Hemisphere transitional VGPs between 97.4°–107.4°/# transitional VGPs.
**Directional groups constructed by Roperch & Duncan (1990) from 66 transitional VGPs, 8 (12 per cent) of which lie between 97.4° and 107.4°.
***See Appendix A.

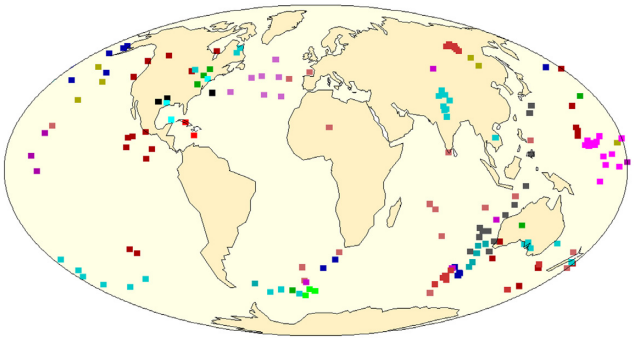

Figure 5. All transitional VGPs from 17 palaeomagnetic records obtained from sites that roughly surround Australasia (see Table 1).

in recognizing aspects of the recorded dynamo reversal process (Hoffman 1984b; Prévot & Camps 1993; Love 1998; Hoffman & Mochizuki 2012)—which we now employ. We define north-VGPs and south-VGPs as follows: north-VGPs are those associated with palaeodirections found in the palaeomagnetic record (i.e. from the rocks). A south-VGP is the antipode to that found in the rocks. That is to say, if, for example, two antipodal VGPs are calculated from palaeodirections found in the same rock sequence, both are by definition north-VGPs.

Fig. 6(a) is the geomagnetic-convention plot for the data shown in Fig. 5. Here each north-VGP in the Northern Hemisphere is displayed by its antipode in the Southern Hemisphere, that is, by its south-VGP equivalent. North-VGPs found in the Southern Hemisphere are unaffected. As can be seen, this procedure adds a significant number of VGPs to the Southern Hemisphere and, in particular, to the virtual pole grouping in the vicinity above the NAD-field flux concentration beneath Australia.

In contrast to past studies, we employ an analytical procedure that does *not* tally the number of clusters present at a given location nor the total number of transitional VGPs contained within each cluster. Rather, our approach is to count the number of Southern Hemisphere blue-region *records* involved at a location, followed by an analysis of the distribution by means of a 10°-wide window of longitude. Fig. 6(b) shows a plot of the number of records having one or more transitional VGPs (i.e. having latitude between 60°S and 0°) in each of the thirty-six 10°-wide longitudinal strips about the globe.

We focus attention now on the 10°-wide longitudinal strip we found to contain transitional virtual poles associated with the largest number of blue-region site records. This band, centred along longitude 102.4°E and highlighted in yellow in Fig. 6(b), contains transitional VGPs from 10 of the 17 records. Although each longitudinal band comprises just 2.8 per cent of global coverage between 60°S and the equator, more than half of the available blue-region

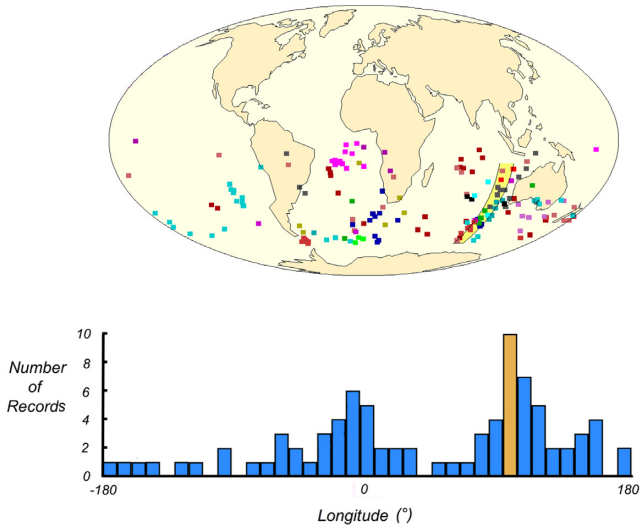

Figure 6. Top: all transitional VGPs contained in 17 palaeomagnetic records from sites shown in Fig. 3 employing the geomagnetic convention. Each is uniquely colour-coded (see Table 1). Bottom: graph of the number of records having at least one VGP for each 10°-wide band of longitude about the Earth. The most populated band centred on longitude 102.4°E is highlighted.

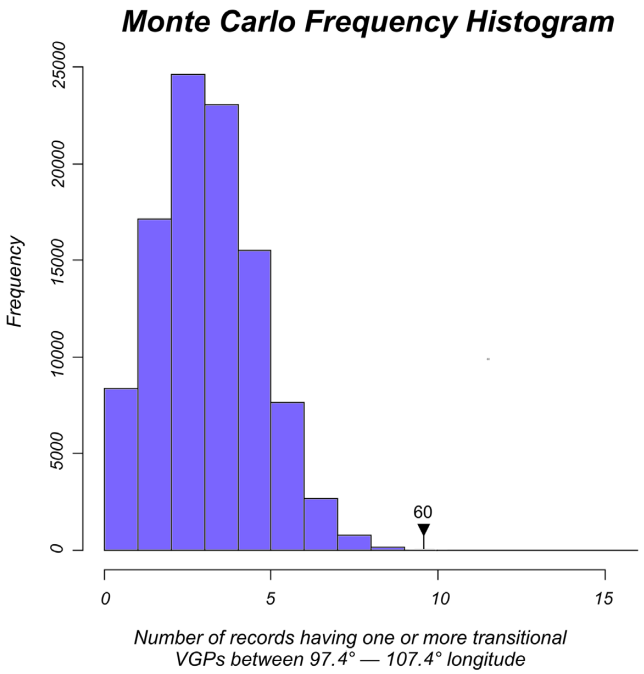

Figure 7. Monte Carlo results: given the number of transitional VGPs displayed for each of the 17 records listed in Table 1, the frequency of occurrence is shown as a function of the number of records having at least one virtual pole within a 10°-wide longitudinal band (100 000 runs). For 10 records, only 60 Monte Carlo runs give such a result (p-value = 0.0006).

site data sets from the Southern Hemisphere are represented in this one narrow strip.

The significance of this finding depends largely on the number of transitional VGPs contained in each individual record in the analysis. While 2 of the records contain between 23–26 VGPs and 5 of the records contain between 13–17 VGPs, the remaining 10, 59 per cent of the records, contain between just 2–7 transitional VGPs and 5 of these 10 'short' records contain at least one VGP within that particular 10°-wide band.

The Monte Carlo method was implemented in the R statistical software environment (R Core Team 2013) to determine the empirical probability of obtaining such a distribution given the number of transitional VGPs in each of the analysed records. The simulation's null hypothesis is that, for a record with n VGPs, the number that appear in any particular 10°-wide longitudinal band can be modelled by a binomial probability distribution with sample size n and success probability 1/36 (since 10° = 1/36 of a circle). That is, the null hypothesis assumes that VGPs are equally likely to occur around the globe. Treating the 17 field records as independent observations, the Monte Carlo simulation recorded how many of those records would include at least one VGP in a specific 10° band under the assumed binomial model (see Appendix B for further details).

Of 100 000 Monte Carlo repetitions, only 60 resulted in ten or more of the 17 field records detecting transitional VGPs within any 10°-wide longitudinal band (p-value = 0.0006, or 0.06 per cent 'successes'), indicating statistically how highly unusual is this finding, regardless of the fact that the site distribution is not spatially uniform. Fig. 7 shows the corresponding Monte Carlo frequency diagram, where the most probable outcome is just 3–4 such records.

It is tempting to conclude from this result that features of the magnetic flux pattern at the CMB—observed in the palaeomagnetic record when the axial dipole had significantly weakened—have remained virtually stationary from the modern-day (Fig. 1) through much of the Cenozoic. However, on further examination one sees an asymmetry in the data—a bias by transitional records from the Plio-Pleistocene. Specifically, there are 11 such records, leaving just 6 older records spanning a significant time range from 9 Ma to nearly 40 Ma. We applied the Monte Carlo technique to each of these two separate groups of data. The 11 younger records (Fig. 8, top) strongly support the initial conclusion: of the 100 000 runs, only 258 (less than 0.3 per cent 'successes') were found to lie in a 10° longitudinal band. Again, a highly unlikely result. The 6 older records (Fig. 8, bottom), however, do not satisfy such a conclusion: of the 100 000 runs 9876 (nearly 10 per cent 'successes') were found to lie in a 10° longitudinal band. Thus, we argue with confidence that the transitional data investigated here support stationarity of CMB primary flux features only through Plio-Pleistocene times—at least during the past 3 Myr.

5 EVIDENCE FROM PALAEOINTESITY DETERMINATIONS

The idea that geomagnetic field intensity may significantly drop during transitional events and that polarity reversals are accompanied by a decrease of 80 or 90 per cent in dipole moment 'is essentially undisputed' (Constable 2007b). If, however, primary NAD-field features along the CMB persist while the strength of the AD field descends during a transitional event, then it is reasonable to suspect that sites at Earth's surface above one of these flux concentrations (see Fig. 1) would initially experience a far less significant reduction in field intensity than would the global average for that latitude. The claim of persistence of the NAD can be tested given robust palaeointensity determinations during transitional times at such a site. Camps *et al.* (2009) report such palaeointensity values for Australian lavas at Liverpool Volcano, New South Wales, Australia, samples that record complex directional field behaviour during the lower portion of the Eocene reversal. Their findings (Fig. 9; Appendix B) associated with 12 flows—5 reverse and 7 transitional, that is, VGP latitudes >60°S and <60°S, respectively—show no

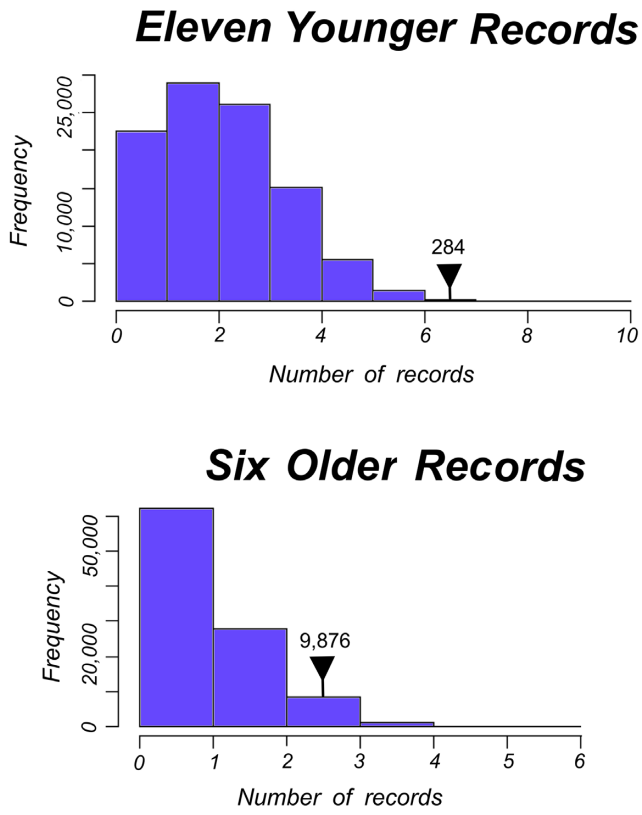

Figure 8. Top: frequency of occurrence as a function of the number of younger records (Pliocene—Quaternary) having at least one virtual pole within a 10°-wide longitudinal band (100 000 runs). Note: 7 of these 11 records contain such a VGP, while the most probable number is two. Only 258 Monte Carlo runs give such a result (p-value = 0.00258). Bottom: frequency of occurrence as a function of the number of older records (Eocene—Miocene) having at least one virtual pole within a 10°-wide longitudinal band (100 000 runs). Note: 3 of these 6 records contain such a VGP, while the most probable number is one. 9876 Monte Carlo runs give such a result (p-value = 0.09876).

obvious sign of any significant intensity decrease. Indeed, the determinations indicate that at least during this significant part of the reversal process the field strength, averaging ∼36 μT, appear more closely aligned with what would be expected during non-transitional times of full polarity.

6 DISCUSSION

The modern-day vertical flux pattern at the CMB (year 1990: Jackson *et al.* 2000) is shown in Fig. 10. Most noteworthy is the striking correspondence between the flux feature extending north-south from high to low latitudes off the west coast of Australia, and the 10°-wide longitudinal strip of Cenozoic transitional VGP seen in Fig. 6(a). This flux feature is also clearly observed from measurements of more recent magnetic survey satellite orbits (e.g. Le Mouël *et al.* 2010). We argue that this surprisingly strong correspondence between Cenozoic transitional fields and the pattern of radial flux presently leaving the outer core provides to date the most significant evidence of tight, long-term mantle control of transitional field morphologies.

Hoffman & Singer (2004) have shown (see their fig. 3) that throughout the 20th century, NAD-field VGPs associated with sites throughout Australasia correlate well with the CMB flux feature off the west coast of Australia. Indeed, the distribution of modern-day NAD-field VGPs from these sites is astonishingly similar to the narrow longitudinal strip of dense transitional VGPs from the Cenozoic.

Expanding on the modern-day NAD-field VGP analysis to sites spanning the globe, the correlation strengthens: Fig. 11 shows the modern-day NAD-field VGP pattern associated with 1368 sites about the globe between latitudes 45°N and 45°S where it is seen that the majority of virtual poles are found along a well-focused, sub-longitudinal band passing along the west coast of Australia and continuing northward. This finding supplies further evidence that the Southern Hemisphere flux feature observed today at the CMB (Fig. 10) has been a major contributor to the global NAD-field over a significant span of geologic time.

These findings also suggest that the observation of 'preferred' VGP pathways (Laj *et al.* 1991) is a phenomenon not altogether caused by longitudinal migration of mobile flux patches at the top of the core, as was first posited by Gubbins & Coe (1993). Rather, the similarity in the pattern of Cenozoic transitional VGPs (Fig. 4), and modern-day NAD-field VGPs associated with the same sites (Fig. 3), suggests that such field behaviour during geomagnetic reversals and events is a consequence of competition among fixed magnetic sources. That is, these pathways may be due to a simple vector addition of the NAD-rich SCOR field from sources near the core surface, and the AD field from sources mainly generated elsewhere, presumably at further depth. Moreover, the fact that 7 of the 17 blue-region data sets (Table 1) are not records of polarity transitions, but rather geomagnetic excursions and events, provides additional evidence that the same dynamo process is at work regardless of whether or not a triggered event culminates in a change of polarity. Hence, such incomplete events may best be considered aborted reversals (e.g. Hoffman 1981; Valet *et al.* 2008).

In summary, our findings strongly suggest that the NAD field is largely a consequence of mantle-held flux anomalies at the core surface, and rather than vanishing with the axial dipole, appears to dominate the global transitional field during reversal attempts. If so, then the suggestion by Hoffman & Singer (2008) that the primary source(s) of the AD field are in some manner separated from those responsible for the NAD (see also Constable 1992; Hoffman 1992; Camps & Prévot 1996) becomes an appropriate issue to explore:

Terms arrived at through spherical harmonic analyses of Earth's magnetic field can be separated into two distinct categories, the so-called dynamo families (Roberts & Stix 1972). The Primary Dynamo Family (E_A) is associated with components of the field that are antisymmetric about the equator, and the Secondary Dynamo Family (E_S) is associated with components of the field that are symmetric about the equator. McFadden *et al.* (1991) showed that full-polarity palaeomagnetic dispersion data recorded about the globe could be analysed so as to quantify the relative importance to palaeosecular variation by each of the two families. What the authors found was that the variability in the E_S/E_A ratio positively correlated with reversal frequency since the Cretaceous Long Normal period. This claim has been strongly challenged by Biggin *et al.* (2008) and quite recently by Doubrovine *et al.* (2019). However controversial, when considered along with the results of this study, we argue that McFadden *et al.*'s suggestion that the degree of interaction between members of the two dynamo families is key to understanding the triggering process for dynamo reversal is worthy of further investigation.

Theory has it that the two families can act separately only under certain idealized conditions. However, these conditions for non-interaction are hypothetical and apparently unrealistic, for example, the mean velocity field of the core fluid must be symmetric,

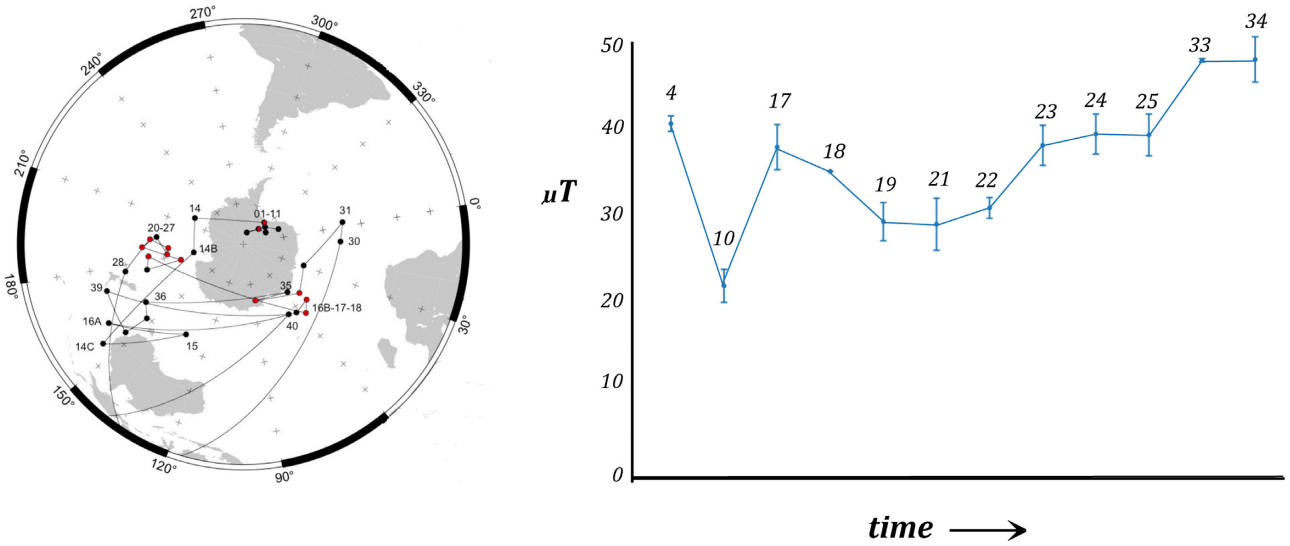

Figure 9. Southern Hemisphere VGPs during the lower portion of the Liverpool reversal (at left) along with determinations of palaeointensity in chronological order (at right). Flow numbers are shown. Note the near complete lack of expected, weak transitional field strengths at the Liverpool site (data from Camps *et al.* 2009).

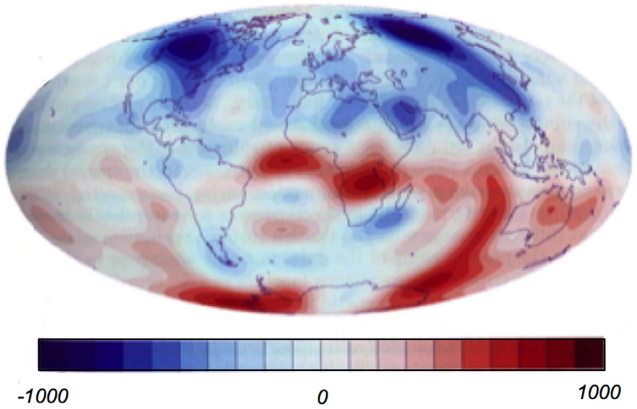

Figure 10. The vertical geomagnetic field at the core–mantle boundary for the year 1990 (Jackson *et al*. 2000, figure 8). Deepness in shade correlates with field strength. Red and blue denote upward- and downward-directed field lines, respectively. Contour interval is 100 μT. Note that the intense flux feature beneath Australia' s west coast correlates with the narrow longitudinal band of transitional VGPs highlighted in Fig. 6.

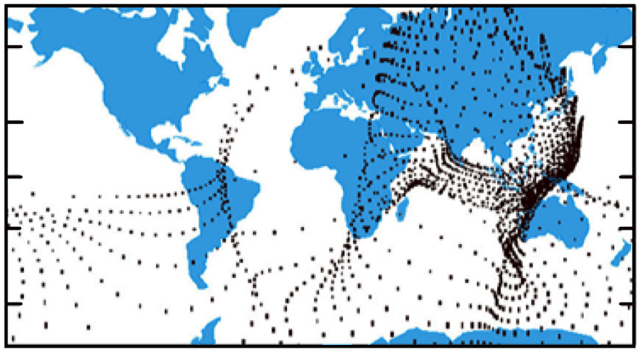

Figure 11. The pattern of modern-day NAD-field south VGPs associated with 1368 sites between 45°N and 45°S latitudes about the globe.

and therefore, non-turbulent (see Jacob 1994). Hence, although the palaeomagnetic dynamo family-related dispersion data are intriguing, it is difficult to explain how members of the E_S family can trigger an attempted field reversal—unless the source of the bulk strength of each family is physically distinct.

By definition, the NAD field contains the entire membership of the Secondary Dynamo Family along with all Primary Family members apart from its most important term, the axial dipole. How then the morphology of fluid flow at depth containing axial dipole flux adjusts to changing thermally induced energetic conditions may determine the degree of interaction with shallow core flux. Therefore, if the NAD field is in some manner the product of flux manipulation in the shallow core by the lowermost mantle, and as suggested by Hoffman & Mochizuki (2012), reverses polarity at a different time from that of the axial dipole, then it follows that times of strong interaction between shallow core flux and deeper-sourced AD-flux may be the initial stage of an attempt by the dynamo to reverse polarity.

7 CONCLUSION

For the case of the Southern Hemisphere, we have shown that both the modern-day NAD-field pattern and palaeomagnetic transitional field data obtained from sites spanning a sizable region of the hemisphere are linked to the most significant vertical flux anomaly emanating today from the fluid core. This anomaly, and hence the associated NAD-field pattern, we argue, owe their existence to some form of flux manipulation brought about by heterogeneities in the shallow-most part of the core. The presented data indicate that this flux feature at the CMB has remained stationary for at least the past 3 Myr, and that it has regionally dominated the remaining field when the axial dipole has significantly weakened during attempts by the dynamo to reverse polarity. Available palaeointensity determinations during a time of transitional field behaviour experienced at an appropriate site are consistent with this claim.

Since the NAD field is comprised by the entire membership of the 'Secondary' (symmetric field) dynamo family, while excluding the most important component of the 'Primary' (antisymmetric

field) dynamo family—the axial dipole—this palaeomagnetic study provides further evidence consistent with the view that the source of the NAD is independent from that which generates the bulk of axial dipole flux. If so, we suggest that such a two-tiered system may be a key element in the complete understanding of dynamo reversal initiation.

ACKNOWLEDGEMENTS

We thank Pavel Doubrovine and Roman Leonhardt for insightful reviews of the original manuscript. KAH wishes to thank the National Science Foundation for its continued support through grant #EAR1015360.

REFERENCES

Biggin, A.J., van Hinsbergen, D.J.J., Langereis, C.G., Straathof, G.B. & Deenen, M.H.L., 2008. Geomagnetic secular variation in the Cretaceous Normal Superchron and in the Jurassic, *Phys. Earth planet. Int.,* **169,** 3–19.

Bogue, S.W. & Coe, R.S., 1984. Transitional palcointensities from Kauai, Hawaii, and geomagnetic reversal models, *J. geophys. Res.,* **89,** 10341–10354.

Bogue, S.W., Glen, J.M.G. & Jarboe, N.A., 2017. Directional change during a Miocene R-N geomagnetic polarity reversal recorded by mafic lava flows, Sheep Creek Range, north central Nevada, USA, *Geochem. Geophys. Geosyst.,* **18,** 3470–3488.

Brown, L., Singer, B.S., Pickens, J. & Jicha, B., 2004. Transitional magnetic field geometry during the Matuyama-Brunhes reversal: paleomagnetic and geochronologic data from the Tatara-San Pedro volcanic complex, Chilean Andes, *J. geophys. Res.,* **109,** doi: 10.1029/2004JB003007.

Camps, P., Perrin, M., Hoffman, K.A. & Singer, B.S., 2009. The LIVERPOOL geomagnetic polarity reversal: new evidence for a complex magnetic field behavior during reversals, *Geophysical Research Abstracts,* **11,** EGU2009–10232.

Camps, P., Henry, B., Prévot, M. & Faynot, L., 2001. Geomagnetic paleosecular variation recorded in Plio-Pleistocene volcanic rocks from Possession Island (Crozet Archipelago, southern Indian Ocean), *J. geophys. Res.,* **106** (B2), 1961–1971.

Camps, P. & Prévot, M., 1996. A statistical model of the fluctuations in the geomagnetic field from paleosecular variation to reversal, *Science,* **273,** 776–779.

Carvallo, C., Camps, P., Ruffet, G., Henry, B. & Poidras, T., 2003. Mono Lake or Laschamp geomagnetic event recorded from lava flows in Amsterdam Island (southeastern Indian Ocean), *Geophys. J. Int.,* **154,** 767–782.

Cassidy, J., 2006. Geomagnetic excursion captured by multiple volcanoes in a monogenetic field, *Geophys. Res. Lett.,* **33,** L21310, doi:10.1029/2006GL027284.

Chauvin, A., Roperch, P. & Duncan, R.A., 1990. Records of geomagnetic reversals from volcanic islands of French Polynesia, 2, paleomagnetic study of a flow sequence (1.2–0.6 Ma) from the island of Tahiti and discussion of reversal models, *J. geophys. Res.,* **95,** 2727–2752.

Constable, C., 1992. Link between geomagnetic reversal paths and secular variation of the field over the last 5 Myr, *Nature,* **358,** 230–233.

Constable, C.G., 2007a. Nondipole field, in *Encyclopedia of Geomagnetism and Paleomagnetism,* pp. 701–704, eds Gubbins, D.G. & Herrero-Bervera, E., Springer.

Constable, C.G., 2007b. Dipole moment variation, in *Encyclopedia of Geomagnetism and Paleomagnetism,* pp. 159–161, eds Gubbins, D.G. & Herrero-Bervera, E., Springer.

Courtillot, V., Valet, J.-P., Hulot, G. & Le Mouël, J.-L., 1992. The Earth's magnetic field: which geometry? *EOS, Trans. Am. geophys. Un.,* **73,** 337–342.

Cox, A. & Hart, R.B., 2009. *Plate Tectonics: How It Works,* Wiley-Blackwell, p. 416.

Doubrovine, P.V., Veikkolainen, T., Pesonen, L.J., Piispa, E., Ots, S., Smirnov, A.V., Kulakov, E.V. & Biggin, A.J., 2019. Latitude dependence of geomagnetic paleosecular variation and its relation to the frequency of magnetic reversals: observations from the Cretaceous and Jurassic, *Geochem. Geophys. Geosyst.,* **20,** 1240–1279.

Dziewonski, A. & Woodhouse, J., 1987. Global images of the Earth's interior, *Science,* **236,** 37–48.

Gubbins, D.R. & Coe, R.S., 1993. Longitudinally confined geomagnetic reversal paths from non-dipolar transition fields, *Nature,* **362,** 51–53.

Hoffman, K.A., 1981. Palaeomagnetic excursions, aborted reversals and transitional fields, *Nature,* **294,** 67–69.

Hoffman, K.A., 1984a. A method for the display and analysis of transitional paleomagnetic data, *J. geophys. Res.,* **89,** 6285–6292.

Hoffman, K.A., 1984b. Geomagnetic reversals, *Nature,* **309,** 90–91.

Hoffman, K.A., 1986. Transitional field behavior from southern hemisphere lavas: evidence for two-stage reversals of the geodynamo, *Nature,* **320,** 228–232.

Hoffman, K.A., 1992. Dipolar reversal states of the geomagnetic field and core–mantle dynamics, *Nature,* **359,** 789–794.

Hoffman, K.A. & Mochizuki, N., 2012. *Geophys. Res. Lett.,* **39,** L06303, doi:10.1029/2011GL050830.

Hoffman, K.A. & Singer, B.S., 2004. Regionally recurrent paleomagnetic transition fields and mantle processes, in *Timescales of the Paleomagnetic Field,* **Vol. 145,** pp. 233–243, eds Channell, J.E.T., Kent, D.V., Lowrie, W. & Meert, J.G., AGU, Geophysical Monograph . American Geophysical Union, doi:10.1029/145GM17.

Hoffman, K.A. & Singer, B.S., 2008. *Science,* **321**, 1800, doi:10.1126/science.1159777.

Hoffman, K.A., Singer, B.S., Camps, P., Hansen, L.N., Johnson, K.A., Clipperton, S. & Carvallo, C., 2008. Stability of mantle control over dynamo flux since the mid-Cenozoic, *Phys. Earth planet. Inter.,* **169,** 20–27.

Jackson, A., Jonkers, A. & Walker, M., 2000. Four centuries of geomagnetic secular variation from historical records, *Phil. Trans. R. Soc. Lond., A,* **358,** 957–990.

Jacobs, J.A., 1994. *Reversals of the Earth's Magnetic Field,* 2nd edn, Cambridge Univ. Press, p. 346.

Koelemeijer, P., Deuss, A. & Ritsema, J., 2017. Density structure of Earth's lowermost mantle from Stoneley mode splitting observations, *Nat. Commun.,* **8,** 15241, doi:10.1038/ncomms15241.

Kustowski, B., Ekström, G. & Dziewonski, A.M., 2008. The anisotropic shear-wave velocity structure of the Earth's mantle: a global model, *J. geophys. Res.,* **113,** 1390, doi:10.1029/2007JB005169.

Laj, C., Mazaud, A., Weeks, R., Fuller, M. & Herrero-Bervera, E., 1991. Geomagnetic reversal paths, *Nature,* **351,** 447, doi:10.1038/351447a0.

Le Mouël, J.L., Shebalin, P. & Khokhlov, A., 2010. Earth magnetic field modeling from Oersted and Champ data, *Earth Planets Space,* **62,** 277–286.

Leonhardt, R., McWilliams, M., Heider, F. & Soffel, H.C., 2009. The Gilsá excursion and the Matuyama/Brunhes transition recorded in 40Ar/39Ar dated lavas from Lanai and Maui, Hawaiian Islands, *Geophys. J. Int.,* **179,** 43–58.

Love, J.J., 1998. Palcomagnetic volcanic data and geometric regularity of reversals and excursions, *J. geophys. Res.,* **103,** 12435–12452.

McFadden, P.L., Merrill, R.T., McElhinny, M.W. & Lee, S., 1991. Reversals of the Earth's magnetic field and temporal variations of the dynamo families, *J. geophys. Res.,* **96,** 3923–3933.

Mochizuki, N., Oda, H., Ishizuka, O., Yamazaki, T. & Tsunakawa, H., 2011. Paleointensity variation across the Matuyama-Brunhes polarity transition: observations from lavas at Punaruu Valley, Tahiti, *J. geophys. Res.,* **116,** B06103, doi:10.1029/2010JB008093.

Plenier, G., Camps, P., Henry, B. & Nicolaysen, K., 2002. Palaeomagnetic study of Oligocene (24-30 Ma) lava flows from the Kerguelen Archipelago (southern Indian Ocean): directional analysis and magnetostratigraphy, *Phys. Earth planet. Inter.,* **133,** 127–146.

Prévot, M. & Camps, P., 1993, Absence of preferred longitude sectors for poles from volcanic records of geomagnetic reversals, *Nature,* **366,** 53–57.

Prévot, M., Mankinen, E.-A., Grommé, C.S. & Coe, R.S., 1985. How the geomagnetic field vector reverses polarity, *Nature,* **316,** 230–234.

R Core Team., 2013. *R: A Language and Environment for Statistical Computing,* R Foundation for Statistical Computing, http://www.R-project.org/.

Riisager, J., Riisager, P. & Pedersen, A.K., 2003. The C27n-C26r geomagnetic polarity reversal recorded in the west Greenland flood basalt province: How complex is the transitional field? *J. geophys. Res.,* **108,** doi:10.1029/2002JB002124.

Ritsema, J., Deuss, A., van Heijst, H.J. & Woodhouse, J.H., 2011. S40RTS: a degree-40 shear-velocity model for the mantle from new Rayleigh wave dispersion, teleseismic traveltime and normal-mode splitting function measurements, *Geophys. J. Int.,* **184,** 1223–1236.

Roberts, P.H. & Stix, M., 1972. α-effect dynamos, by the Bullard-Gellman formalism, *Astron. Astrophys.,* **18,** 453–466.

Roperch, P. & Duncan, R.A., 1990. Records of geomagnetic reversals from volcanic islands of French Polynesia: 1. Paleomagnetic study of a polarity transition in a lava sequence from the Island of Huahine, *J. geophys. Res.,* **95,** 2713–2726.

Schettino, A. & Scotese, C.R., 2005. Apparent polar wander paths for the major continents (200 Ma to the present day): a palaeomagnetic reference frame for global plate tectonic reconstructions, *Geophys. J. Int.,* **163,** 727–759.

Singer, B.S., 2014. A Quaternary geomagnetic instability time scale, *Quat. Geochronol.,* **21,** 29–52.

Tetley, M.G., Williams, S.E., Gurnis, M., Flament, N. & Müller, R.D., 2019. Constraining absolute plate motions since the Triassic, *J. geophys. Res.,* **124**(7), 7231–7258.

Valet, J.-P. & Plenier, G., 2008. Simulations of a time-varying non-dipole field during geomagnetic reversals and excursions, *Phys. Earth planet. Inter.,* **169,** 178–193.

Valet, J.-P., Plenier, G. & Herrero-Bervera, E., 2008. Geomagnetic excursions reflect an aborted polarity state, *Earth planet. Sci. Lett.,* **274,** 472–478.

Yamamoto, Y., Ishizuka, O., Sudo, M. & Uto, K., 2007. 40Ar/39Ar ages and paleomagnetism of transitionally magnetized volcanic rocks in the Society Islands, French Polynesia: Raiatea excursion in the upper-Gauss Chron, *Geophys. J. Int.,* **169,** 41–59.

SUPPORTING INFORMATION

Supplementary data are available at *GJI* online.

Suppl.Online.Mat: Online Supplement (Refer to Table I).

Please note: Oxford University Press is not responsible for the content or functionality of any supporting materials supplied by the authors. Any queries (other than missing material) should be directed to the corresponding author for the paper.

APPENDIX A: PLATE-TECTONIC RECONSTRUCTION METHOD EMPLOYED

The finite rotation poles used to transfer the VGPs into Earth's spin axis reference frame are marked in bold characters in the following table. They are calculated from Schettino & Scotese (2005) and the OptAPM1-M16 reconstruction model of Tetley *et al.* (2019) by means of a global circuit through the central Africa.

To achieve increased accuracy, we interpolated within these models the Euler poles at the age of the volcanic sequences considered in this study. For this purpose, we calculated the stage pole as explained in Cox & Hart (2009, chap. 7) assuming that the rate of motion and the direction of motion do not change within the time interval yielded in the plate motion models. We combined the successive rotations within the global circuit through central Africa into a single rotation by means of matrix multiplications following the properties of the non-abelian group SO(3) (e.g. Cox & Hart 2009).

	Euler pole		
Plate ID/fixed Plate ID	Lat (°)	Long (°)	Angle (°)
Kaputar : Time 18 Ma			
801/802	−15.10	213.17	10.74
802/701	10.36	311.90	2.49
701/001	59.15	−64.44	−4.61
801/001	**−32.92**	**211.74**	**11.63**
Quamby Fall : Time 26.5 Ma			
801/802	−14.47	213.14	16.13
802/701	11.55	311.77	4.10
701/001	55.28	−59.84	−6.81
801/001	**−30.46**	**211.03**	**17.39**
Liverpool : Time 37 Ma			
801/802	−15,45	211.34	22.17
802/701	11.76	313.75	6.33
701/001	49.81	−54.16	−9.21
801/001	**−29.23**	**208.83**	**23.86**
Kerguelen : Time 27 Ma			
802/701	11.60	311.76	4.20
701/001	55.04	−59.64	−6.95
802/001	**−82.44**	**22.55**	**4.92**

Where the plate IDs are—001: present day Atlantic/Indian hotspots; 701: African Craton; 801: Australia; 802: Antarctica and East Antarctica.

APPENDIX B: DETAILS OF THE EMPLOYED MONTE CARLO METHOD

Take the 11 younger flows, for example. Each has a different number of transitional VGPs. For each loop of the simulation, the following was done:

(1) 11 binomial random variables were generated. Each one has an 'n' equal to the number of VGPs in the record; for example, X1 has $n = 14$, X2 has $n = 6$, and so on. All 10 of them use $p = 1/36$, the probability of a VGP falling into the particular 10° window of interest.

(2) The number of binomial random variables ≥ 1 were counted. So, randomly, and with the number of observed VGPs in each record, how many records out of 11 would we expect to show at least one VGP in the 10° window? That count, anything from 0 through 11, is graphed at the top of Fig. 8.

(3) Since 7 of the 11 records had at least one VGP in the window of interest, the (empirical) p-value is the chance of 7 or more binomial random variables of being positive. (For this case, that value turns out to be super-small.)